Sheffield Hallam University

Ultrahigh piezoelectricity in lead-free piezoceramics by synergistic design

WANG, Dawei <http://orcid.org/0000-0001-6957-2494>, FAN, Zhongming, RAO, Guanghui, WANG, Ge, LIU, Yao, YUAN, Changlai, MA, Tao, LI, Dejun, TAN, Xiaoli <http://orcid.org/0000-0002-4182-663X>, LU, Zhilun, FETEIRA, Antonio <http://orcid.org/0000-0001-8151-7009>, LIU, Shiyu, ZHOU, Changrong and ZHANG, Shujun

Available from Sheffield Hallam University Research Archive (SHURA) at:

https://shura.shu.ac.uk/26530/

This document is the Supplemental Material

Citation:

WANG, Dawei, FAN, Zhongming, RAO, Guanghui, WANG, Ge, LIU, Yao, YUAN, Changlai, MA, Tao, LI, Dejun, TAN, Xiaoli, LU, Zhilun, FETEIRA, Antonio, LIU, Shiyu, ZHOU, Changrong and ZHANG, Shujun (2020). Ultrahigh piezoelectricity in lead-free piezoceramics by synergistic design. Nano Energy, 76, p. 104944. [Article]

Copyright and re-use policy

See http://shura.shu.ac.uk/information.html

Sheffield Hallam University Research Archive
http://shura.shu.ac.uk

Supplementary information

Table S1. Refinement parameters of BTSx ceramics by full pattern Rietveld refinements

x	space group	a / Å	b / Å	c / Å	Alfa / °	Fraction / %	GOF	R_{exp}	R_{wp}
0.05	*Amm2*	4.02623(3)	5.66093(4)	5.66313(5)	90	68	1.86	8.04	14.96
	P4mm	4.00639(4)	4.00639(4)	4.02428(4)	90	32			
0.08	*Amm2*	4.00834(6)	5.68834(11)	5.68293(9)	90	47	1.96	7.46	14.67
	P4mm	4.01116(6)	4.01116(6)	4.02122(6)	90	53			
0.11	*Amm2*	4.02003(3)	5.67791(12)	5.67859(13)	90	32	1.71	8.01	13.67
	P4mm	4.01737(3)	4.01737(3)	4.01728(6)	90	25			
	R3m	4.02361(7)	4.02361(7)	4.02361(7)	89.98432(7)	17			
	Pm3m	4.01891(3)	4.01891(3)	4.01891(3)	90	26			
0.14	*Pm3m*	4.02088(4)	4.02088(4)	4.02088(4)	90	86	1.91	6.86	13.1
	R3m	4.03052(8)	4.03052(8)	4.03052(8)	89.99266(2)	14			
0.18	*Pm3m*	4.02495(3)	4.02495(3)	4.02495(3)	90	100	1.96	7.83	15.36

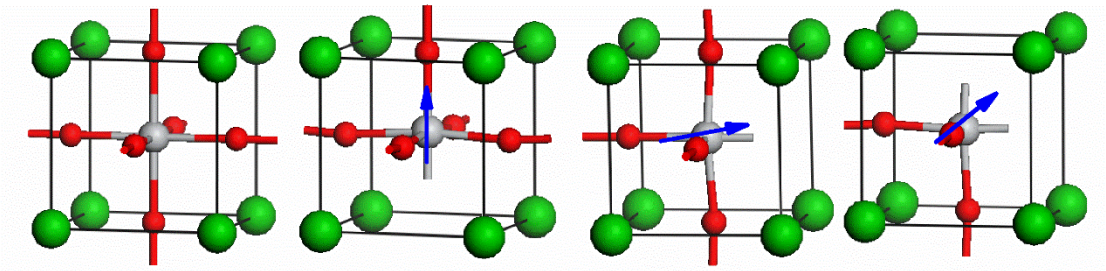

Figure S1. Crystal structures of (a) cubic (C), (b) tetragonal (T), (c) orthorhombic (O), and (d) rhombohedral (R) phase for $BaTiO_3$. The large green, medium gray, and small red balls represent the Ba, Ti, and O atoms, respectively. Blue arrows mark certain directions of polarization vectors in T, O, R phases, respectively.

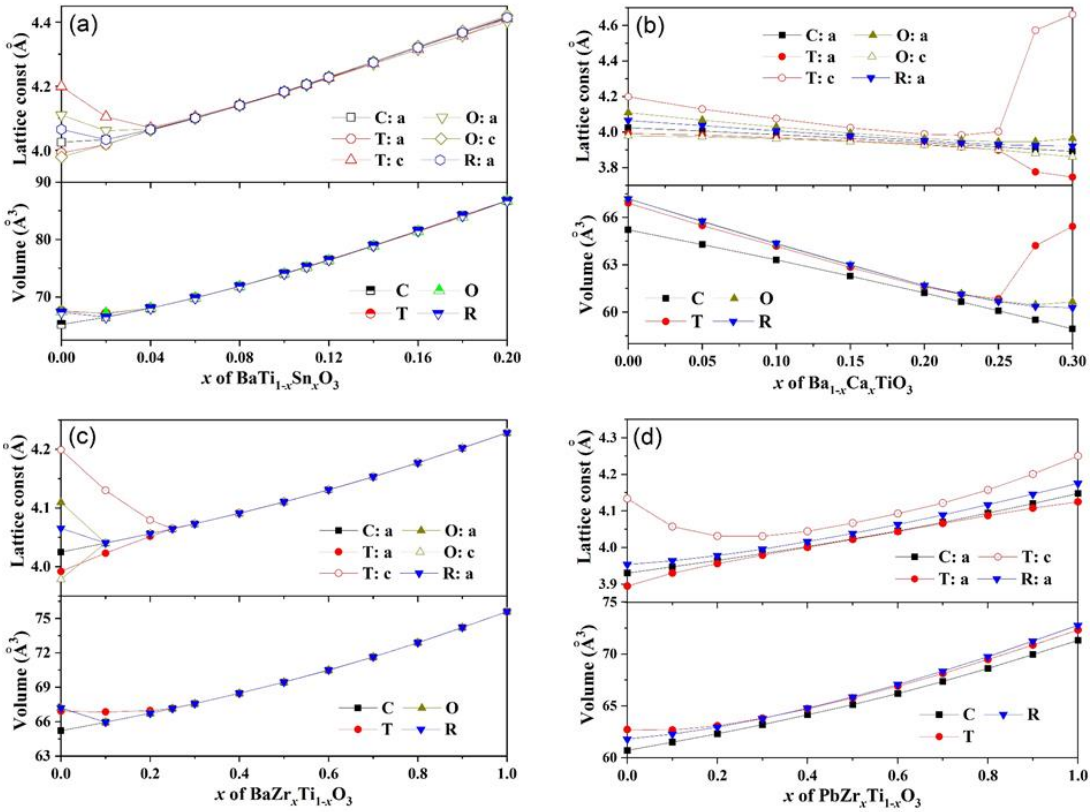

Figure S2. The calculated lattice constants and the volumes properties of cubic (C), tetragonal (T), orthorhombic (O) and rhombohedral (R) phases for (a) $BaTi_{1-x}Sn_xO_3$ ($0 \leq x \leq 0.2$), (b) $Ba_{1-x}Ca_xTiO_3$ (BCxT, $0 \leq x \leq 0.3$), (c) $BaZr_xTi_{1-x}O_3$ (BZT, $0 \leq x_{Zr} \leq 1$) and (d) $PbZr_xTi_{1-x}O_3$ (PZT, $0 \leq x_{Zr} \leq 1$).

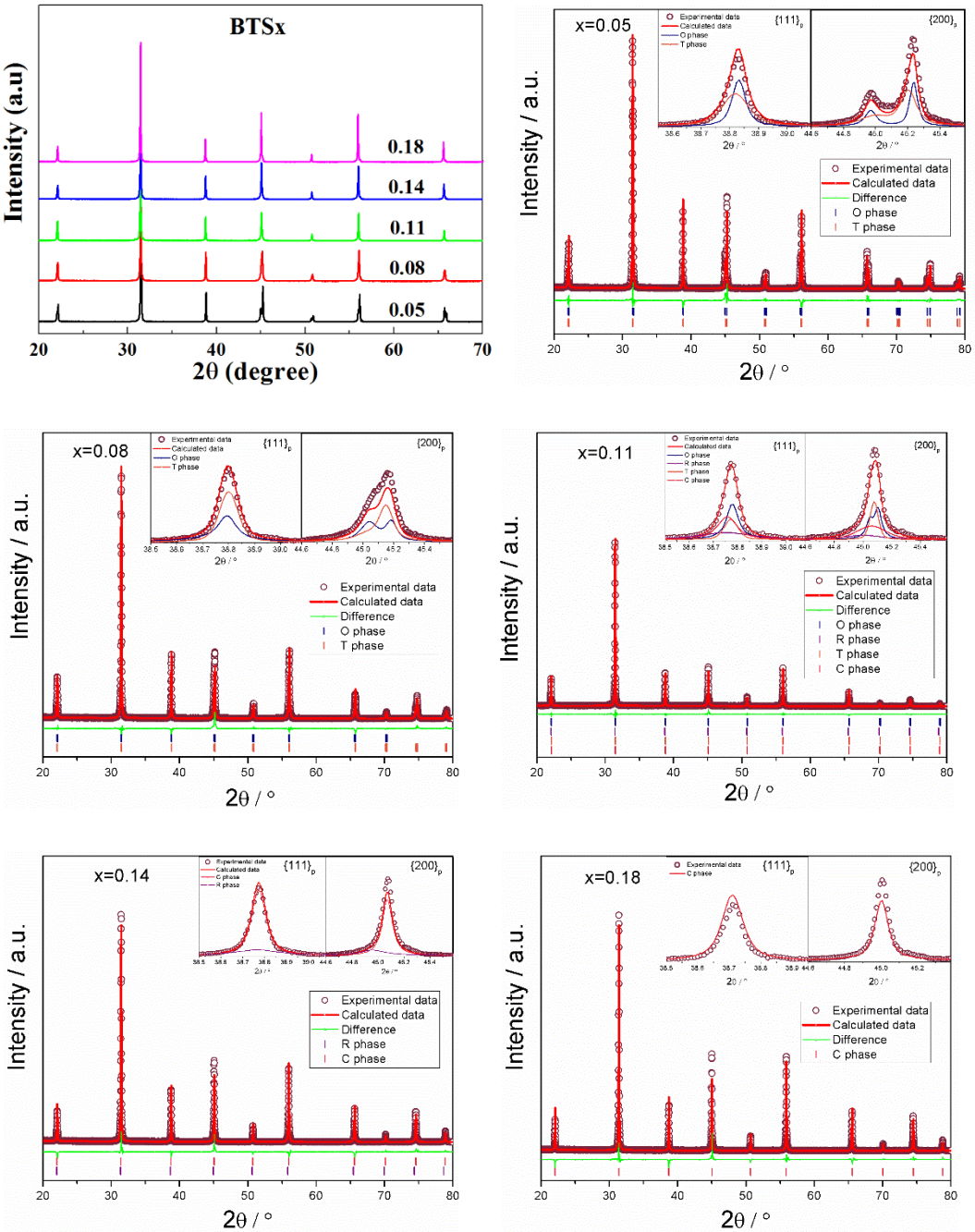

Figure S3. The room temperature XRD patterns of BTSx ceramics and the corresponding results of full pattern Rietveld refinements.

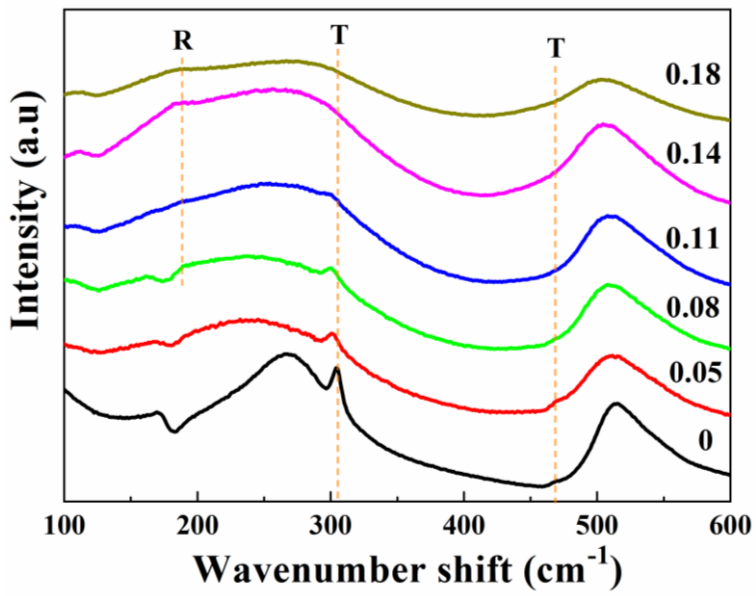

Figure S4. The room temperature Raman spectra of BTSx ceramics

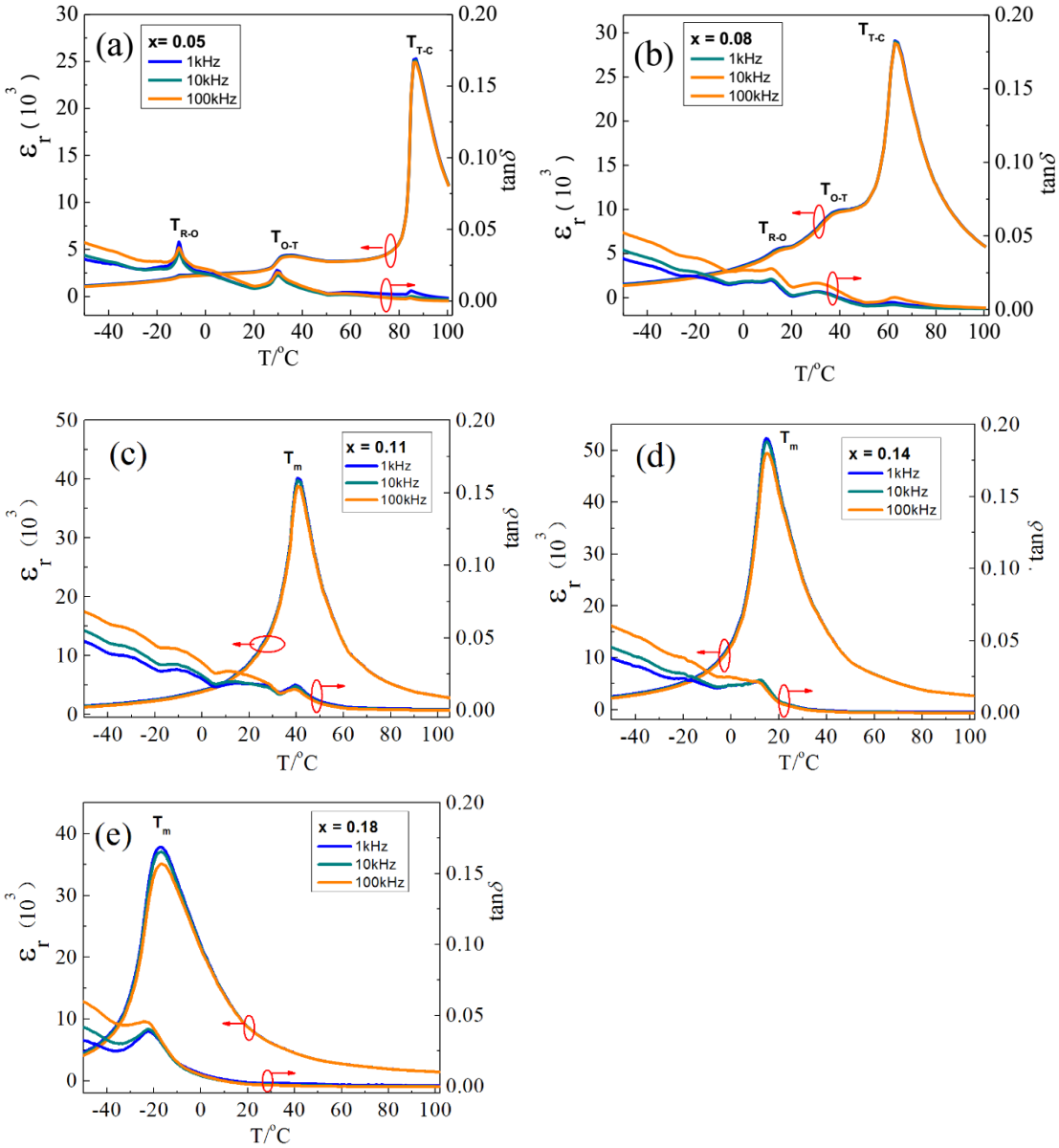

Figure S5. Temperature dependence of the dielectric permittivity (ε_r) and loss (tanδ) for BTSx ceramics

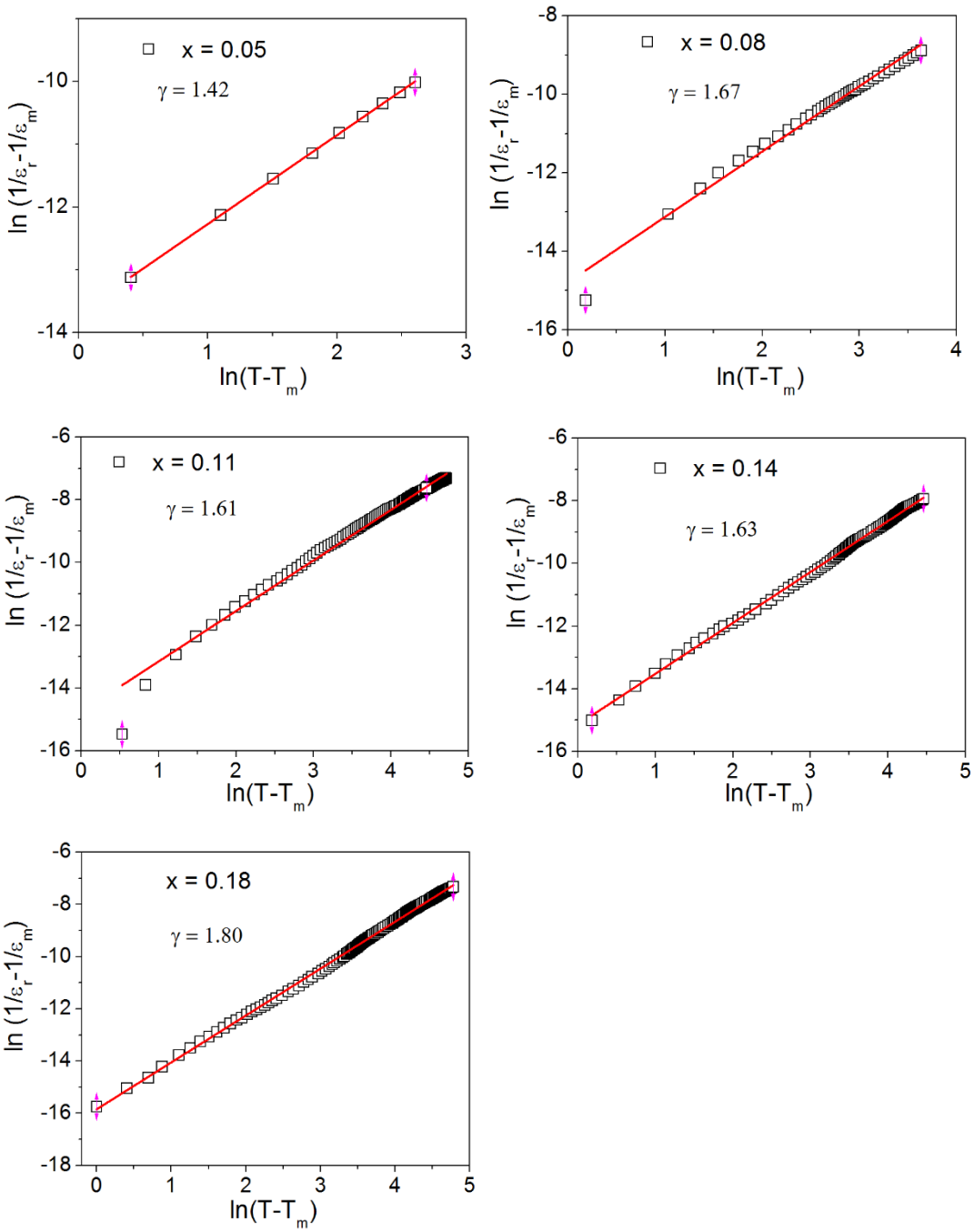

Figure S6. $\ln(1/\varepsilon_r - 1/\varepsilon_{max})$ as a function of $\ln(T-T_m)$ at 10 kHz for BTSx ceramics.

The modified Curie-Weiss law, $(1/\varepsilon_r - 1/\varepsilon_{max}) = C^{-\gamma} (T-T_m)^{\gamma}$, where C is the Curie coefficient, ε_{max} is the maximal dielectric constant, T_m is the temperature of ε_{max}, γ is the degree of diffuseness

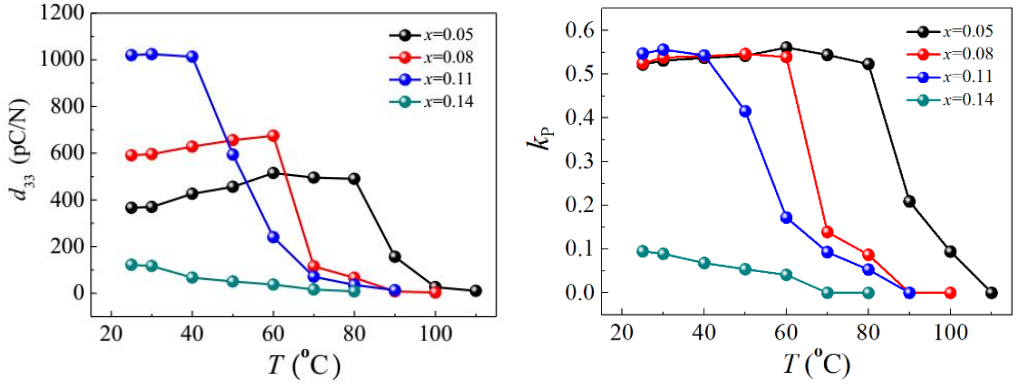

Figure S7. The *ex-situ* temperature dependence of d_{33} and k_p for BTSx ceramics.

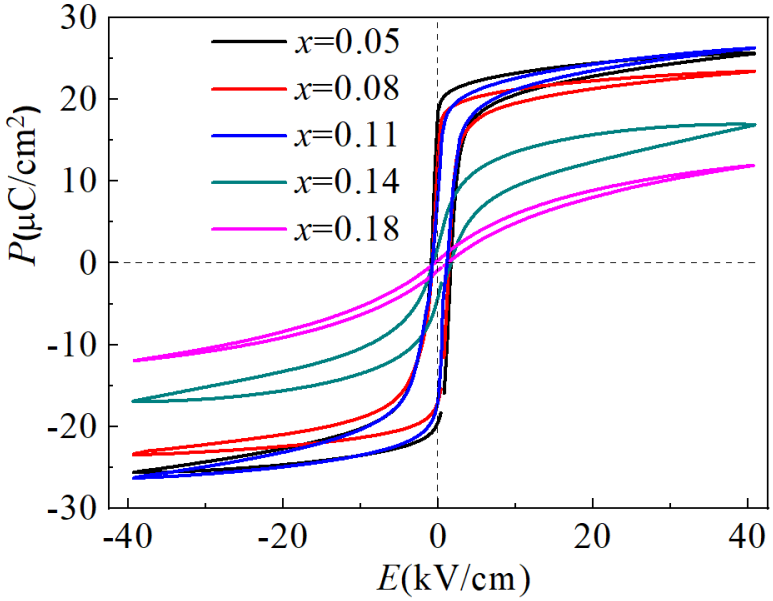

Figure S8. The *P-E* loops for BTSx ceramics.